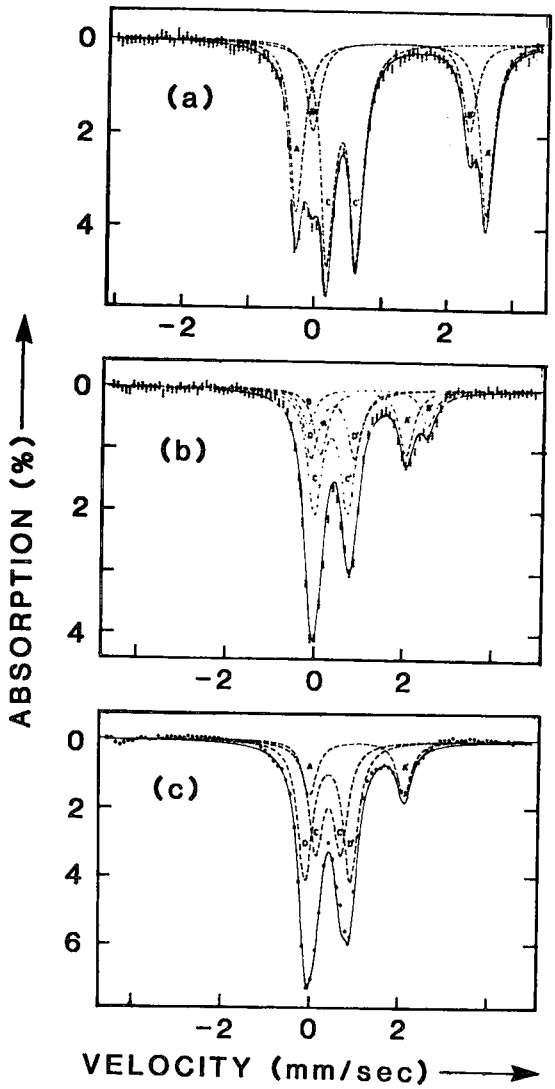

FIG. 105. Mössbauer spectra for natural (top) and heated (bottom) riebeckite [from Ernst & Wai (1970)].

In iron-rich amphiboles, there is insufficient OH to oxidize all the Fe^{2+} by this oxidation–dehydroxylation, and even completely dehydroxylated material contains Fe^{2+}, as shown in Figure 105 for riebeckite{29} (see Appendix F for details). Comparison of the spectra for material heated for 1 hour and 94 hours shows that oxidation of Fe^{2+} still proceeds in the absence of OH, but it is a much slower process with a completely different mechanism. Similarly, in iron-poor amphiboles, dehydroxylation proceeds much more slowly once the oxidation–dehydroxylation mechanism has resulted in complete oxidation of all the Fe^{2+}, but the mechanism of charge compensation (if any) is not known.

Rouxhet *et al.* (1972) examined the progressive oxidation of fibrous grunerite and crocidolite. This process appears to take place continuously over a wide range of temperatures in both materials. In crocidolite, there is a 1:1 correlation between the FeO content and the loss of OH from the sample (measured as the sum of the integrated absorbances of the OH bands), indicating that while OH is present, oxidation proceeds by dehydrogenation. In fibrous grunerite, there is a 3:2 correlation between FeO content and OH content, indicating that dehydrogenation and oxidation occur together (Addison *et al.* 1962a, b, Hodgson *et al.* 1965, Ernst & Wai 1970). Oxidation is accompanied by a loss of tensile strength of the fibres (*e.g.*, Aveston 1969) that "seems to be due to thermal decomposition". When heated under vacuum, oxidation increases with increasing temperature, until it reaches a maximum, above which reduction begins. Below the temperature of maximum oxidation, hydrogen is released by progressive heating; above the temperature of maximum oxidation, oxygen is released. Rouxhet *et al.* (1972) also suggested that the X-ray pattern of crocidolite anhydride reported by Hodgson *et al.* (1965) is actually due to oxy-crocidolite, with crocidolite anhydride being amorphous.

Some preliminary structure-refinement results on oxidized amphiboles have been reported by Ungaretti (1980). Structure refinements before and after heating show a reduction in cell dimensions, considerable shortening of all the bonds to O(3) and disappearance of the H atom in Fourier maps. Of considerable interest is the fact that the oxidation–dehydroxylation process has been accompanied by considerable disordering of cations. In particular, Na has moved from the M(4) site to the A site, leaving vacancies at M(4); this confirms the conclusions drawn from the 3685 cm^{-1} bands in Figure 103. In addition, these results confirm the suggestions of cation reordering over the M(1), M(2) and M(3) sites from the Mössbauer spectra of Figure 104.

HIGH-TEMPERATURE CRYSTALLOGRAPHY

Although a large number of heating studies on amphiboles have been carried out over the past fifty years, these have been concerned mainly with oxidation–dehydroxylation relation-

TABLE 64. THERMAL EXPANSION DATA FOR ACTINOLITE AND HORNBLENDE

	α^*_{11}	α_{22}	α_{33}	Temp. range
Actinolite	0.82	0.92	0.36	-168 to 20°C
	1.22	1.40	0.58	20 to 196°C
Hornblende	0.82	0.78	0.26	-175 to 20°C
	0.78	1.16	0.31	20 to 200°C

Actinolite	$a=9.888(1+7.86\times10^{-6}t+1.67\times10^{-9}t^2)$Å
	$b=18.136(1+10.47\times10^{-6}t+10.24\times10^{-9}t^2)$Å
	$c=5.309(1+8.06\times10^{-6}t+7.19\times10^{-9}t^2)$Å
Hornblende	$a=9.939(1+5.29\times10^{-6}t+1.33\times10^{-9}t^2)$Å
	$b=17.996(1+10.00\times10^{-6}t+10.39\times10^{-9}t^2)$Å
	$c=5.299(1+4.94\times10^{-6}t+1.24\times10^{-9}t^2)$Å

*$\alpha = \alpha\times10^5$. Data from Quadrado & Gutierrez (1967).

TABLE 65. THERMAL EXPANSION DATA FOR TIRODITE $P2_1/m(\overline{27})$ (AT 24°C) AND TIRODITE(41) (AT 270°C)

	24°C	270°C	α^*
a(Å)	9.550(1)	9.595(1)	1.915
b(Å)	18.007(7)	18.077(2)	1.581
c(Å)	5.298(1)	5.307(1)	0.691
β(°)	102.65(1)	102.61(2)	-0.158
V(Å^3)	888.9(2)	898.4(2)	4.344
<T(1)-O>(Å)	1.617	1.617	0.000
<T(2)-O>(Å)	1.625	1.629	1.001
<M(1)-O>(Å)	2.080	2.087	1.368
<M(2)-O>(Å)	2.078	2.084	1.174
<M(3)-O>(Å)	2.073	2.079	1.177
<M(4)-O>(Å)	2.296	2.303	1.239

*$\alpha = \alpha\times10^5$. Data from Sueno *et al.* (1972a).

ships (see previous section) and breakdown reactions. It is only recently that high-temperature crystallographic studies have been carried out on amphiboles. The first work in this field is that of Quadrado & Gutiérrez (1967), who examined the thermal expansion of actinolite and hornblende by Weissenberg methods over the temperature range $-170 \rightarrow 200$°C. The results of these authors are summarized in Table 64. They found a nonlinear thermal expansion over this range, with the thermal expansion increasing with increasing temperature. Table 65 also shows the coefficients of thermal expansion over the temperature intervals $-170 \rightarrow 20$°C and $20 \rightarrow 200$°C; the values for actinolite over the higher-temperature range agree closely with corresponding values for tremolite derived by Sueno *et al.* (1973), as shown in Table 66.

TABLE 66. THERMAL EXPANSION DATA FOR TREMOLITE (30), (53a) AND (53b), POTASSIUM-RICHTERITE (P3), AND RICHTERITE (P4)

		24°C	400°C	600°C	700°C	α^*
Tremolite	a(Å)	9.818(5)	9.860(1)	-	9.898(2)	1.202
	b(Å)	18.047(8)	18.118(3)	-	18.190(3)	1.167
	c(Å)	5.275(3)	5.285(1)	-	5.296(1)	0.583
	β(°)	104.65(5)	104.57(1)	-	104.46(1)	-0.266
	V(Å^3)	904.2(6)	913.8(2)	-	923.4(2)	3.131
Potassium-richterite	a(Å)	9.944(1)	9.988(1)	10.013(1)	-	1.205
	b(Å)	17.972(3)	18.056(2)	18.107(2)	-	1.304
	c(Å)	5.260(1)	5.272(1)	5.278(1)	-	0.594
	β(°)	104.80(1)	104.70(1)	104.64(1)	-	-0.265
	V(Å^3)	908.9(2)	919.7(2)	925.9(2)	-	3.247
Richterite	a(Å)	9.824(2)	9.855(2)	9.883(2)	-	1.043
	b(Å)	17.956(4)	18.036(3)	18.087(2)	-	1.267
	c(Å)	5.258(1)	5.270(1)	5.278(1)	-	0.660
	β(°)	104.23(1)	104.10(1)	104.08(1)	-	-0.250
	V(Å^3)	899.0(3)	908.4(3)	915.2(4)	-	3.128

*$\alpha = \alpha\times10^5$

Deer *et al.* (1963) suggested the existence of cummingtonite $P2_1/m$ as a possible amphibole analogue of pigeonite. Ross *et al.* (1968a, 1969) carried this analogy further and suggested that cummingtonite $P2_1/m$ would invert to a $C2/m$ phase at high temperature. This was demonstrated by Prewitt *et al.* (1970), who showed that a $P2_1/m \rightarrow C2/m$ transition occurred at ~45°C for a cummingtonite of composition $(Ca_{0.36}Na_{0.06}Mn_{0.96}Mg_{0.57})Mg_5Si_8O_{22}(OH)_2$. Sueno *et al.* (1972a) showed that a tirodite $P2_1/m$ inverted to $C2/m$ symmetry at ~100°C, and refined the crystal structure of the $C2/m$ phase at 270°C [tirodite(41)]. The high-temperature structure is very similar to that of tirodite(28); details of both structures are given in Appendix B, and those of the $P2_1/m$ structure are given in Appendix D. Perhaps the most significant aspect of the primitive- to high-cummingtonite transition concerns the degree of kinking of the tetrahedral double-chains. At room temperature, the O(5)–O(6)–O(5) angles are 166.2(4) and 178.4(4)°, respectively, for the B and A chains of the $P2_1/m$ structure. As the temperature increases, the A chain becomes more kinked and the B chain straightens until they become equivalent at the transition. Sueno *et al.* (1972a) suggested that differential thermal expansion of octahedra and tetrahedra is an important factor in this transition. The expansion data are shown in Table 65; note that these disregard any possible discontinuity at the phase transition. With increasing temperature, octahedra expand more rapidly than tetrahedra; hence, increasing temperature affects the structure in a similar way to the substitution of larger cations. The result is a structure very similar to that of tirodite, which has $C2/m$ symmetry.

The importance of the M(4) site and its constituent cations has been emphasized in previous sections, and it is not surprising that some of the most significant changes across the $P2_1/m \rightarrow C2/m$ transition occur at and around

this site. With increasing temperature, the M(4) cation moves away from the octahedral strip toward the position occupied by Ca in the calcic amphiboles; this is compatible with the increased solid-solution between Fe–Mg–Mn amphiboles and calcic amphiboles at higher temperatures that is suggested by the presence of exsolution lamellae in pairs of coexisting amphiboles of these compositions. Another very intriguing aspect is the behavior of the isotropic temperature-factor for the M(4) cation. The increase in B at M(4) is less than that for the M(1), M(2) and M(3) sites, and at room temperature, B of M(4) is larger than B at M(1), M(2) and M(3). Sueno *et al.* (1972a) suggested that the Mn+Mg+Ca at M(4) in cummingtonite $P2_1/m$ are positionally disordered, thus leading to an anomalously large B at M(4); with increasing temperature, the Mn and Mg move toward the Ca position, thus decreasing the positional disorder and decreasing the contribution of the positional disorder to B at the M(4) site and offsetting somewhat the effect of increased thermal vibration due to increasing temperature.

Sueno *et al.* (1973) reported high-temperature X-ray refinements of the structure of tremolite [see tremolite(30), (53a) and (53b) in Appendix B], and Cameron *et al.* (1973a, b) and Cameron & Papike (1979) gave some details of high-temperature X-ray refinements of the structure of fluor-richterite and potassium-fluor-richterite [see fluor-richterite(P2) and potassium-fluor-richterite(P3) in Appendix E]. These three amphiboles all have the same chemical components in the octahedral strip and tetrahedral chain. The thermal-expansion data for these structures are shown in Table 66 and Figure 106; the a and c dimensions show the largest

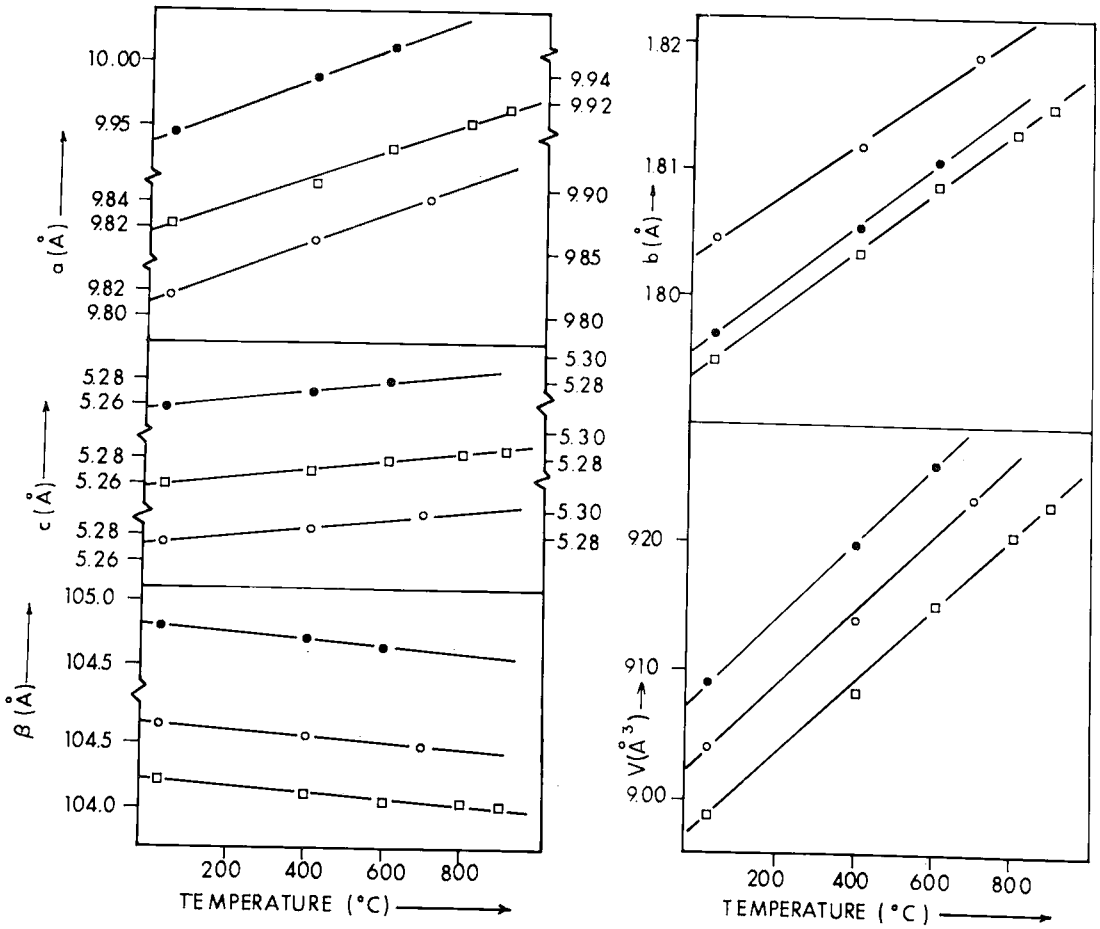

FIG. 106. Variation of cell dimensions as a function of temperature for tremolite (○), fluor-richterite (□) and potassium-fluor-richterite (●) [after Cameron & Papike (1979)].

and smallest mean thermal-expansion coefficients, respectively. Sueno *et al.* (1973) contrasted the thermal-expansion behavior of tremolite with that of diopside (Cameron *et al.* 1973c), whose *b* dimension has the largest mean thermal-expansion coefficient; in tremolite(30), the A site has a large mean thermal-expansion coefficient, resulting in the large value of this parameter in the *X* direction. Expansion along *Z* is controlled in part by the straightening of the double chains of relatively inert silicate tetrahedra. The small amount of chain straightening, coupled with the negligible increase in size or distortion of the tetrahedra, results in a "clamping effect" on expansion of the octhedral strip in the *Z* direction. Similar arguments may be applied to the parallel behavior of richterite (Fig. 106). The relative displacement of the back-to-back tetrahedral chains strongly affects the anion arrangement about the M(4) site [*cf.* Hawthorne & Grundy (1977c) and Hawthorne & Calvo (1977) for the analogous situation in pyroxenes]; increasing temperature increases this displacement, whereas increasing M(4) cation size decreases this displacement. Sueno *et al.* (1973) showed that chain displacement is positively correlated with the "co-ordination coefficient" of M(4), a measure of the dispersion of the M(4)–O distances. Thus the M(4) cation tends to become more six-co-ordinated with increasing temperature; note that this tends to promote increased solid-solution with Fe–Mg–Mn amphiboles at higher temperatures.

The high-temperature structure-refinements for tirodite(41) and tremolite(53a) and (53b) show marked differential polyhedral expansion with increasing temperature (see Appendix B3), a feature that is also exhibited by the two specimens of fluor-richterite (P2) and P(3) (Cameron & Papike 1979). The silicate tetrahedra are virtually unaffected by increasing temperature, with no significant increases in either mean bond-length or bond angles. However, the remaining polyhedra show significant increases in mean bond-lengths that are linear with temperature (Fig. 107), although the bond angles are only slightly changed, except where affected by differential polyhedral expansion. Thus with increasing temperature, the elements in the octahedral strip show considerable thermal expansion as a result of expansion of the individual octahedra, an effect that is not present in the double-chain element. This produces a potential misfit between the two elements that is accommodated by a straightening of the tetrahedral double-chain, together with a tilting of the tetrahedra (Fig. 108); the effects involved here are *similar* to those involved in accommodation of the two structure elements with variable chemical composition.

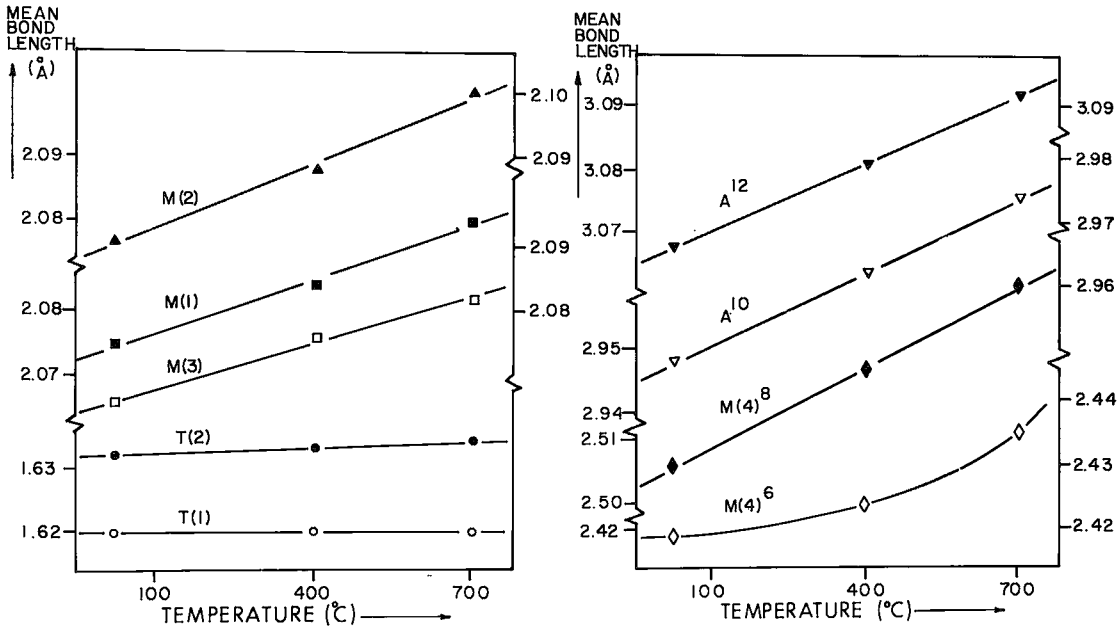

FIG. 107. Variation in mean bond-lengths as a function of temperature for tremolite(30), (53a) and (53b) [after Cameron & Papike (1979)].

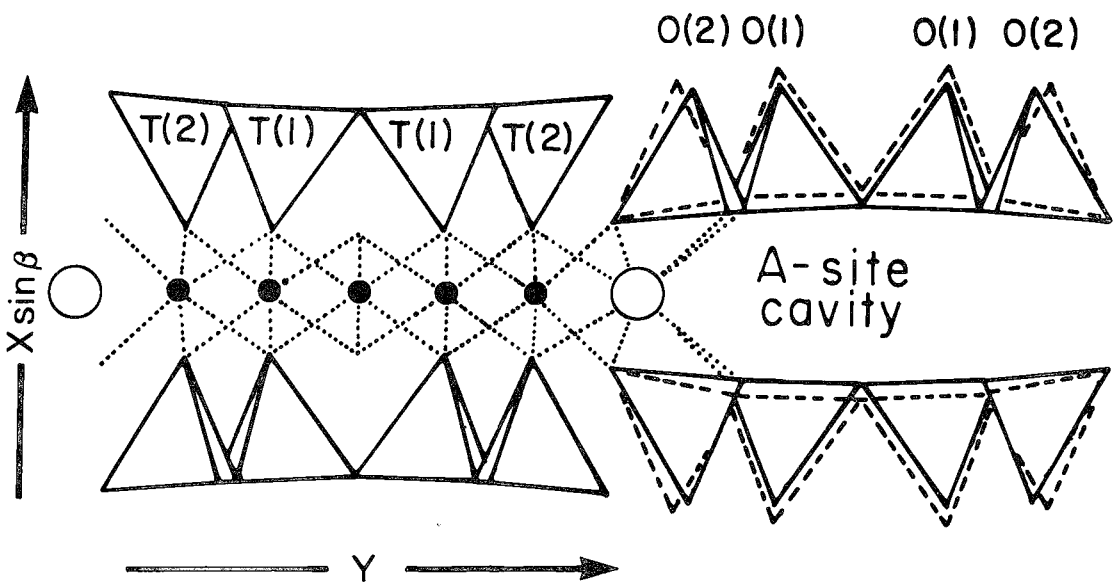

FIG. 108. The room-temperature crystal structure of tremolite projected down *Z*. The dashed lines associated with the tetrahedral double-chains show their movement (highly exaggerated) with increasing temperature [after Sueno *et al.* (1973)].

In tremolite, the increase in equivalent isotropic temperature-factors for all ions at all sites is linear with temperature (Sueno *et al.* 1973). The observed values and the rates of increase are approximately the same for identical cations (Table 67), and seem to be inversely related to the mean bond-valence in the co-ordination polyhedron. For the anions, both the magnitudes and the rates of increase with temperature are inversely related to the co-ordination number of the anion. The overall behavior of the thermal vibration model of tremolite is very similar to that of diopside (Cameron & Papike 1981).

TABLE 67. VARIATION OF EQUIVALENT ISOTROPIC TEMPERATURE FACTORS (Å^2) WITH TEMPERATURE DERIVED FROM HIGH-TEMPERATURE CRYSTAL-STRUCTURE REFINEMENTS

	Tremolite				Tirodite		
	(30)	(56a)	(56b)		($\bar{2}7$)	(41)	
	24°C	400°C	700°C	C.N.	24°C	270°C	C.N.
O(1)	0.35(3)	1.02(4)	1.49(6)	4	0.41	1.07(6)	4
O(2)	0.39(3)	1.06(4)	1.52(6)	4	0.46	0.97(6)	4
O(3)	0.46(4)	1.26(6)	1.79(8)	3	0.48	0.93(8)	3
O(4)	0.51(3)	1.42(5)	2.02(6)	3	0.67	1.50(7)	3
O(5)	0.46(3)	1.26(5)	1.88(6)	3	0.60	1.37(3)	2,3
O(6)	0.45(3)	1.29(5)	1.81(6)	3	0.89	1.46(7)	3
O(7)	0.50(4)	1.39(7)	2.18(9)	2	0.89	1.34(9)	2
T(1)	0.19(1)	0.77(2)	1.07(3)	4	0.27	0.78(2)	4
T(2)	0.19(1)	0.77(2)	1.11(3)	4	0.30	0.88(2)	4
M(1)	0.33(2)	1.02(3)	1.38(4)	6	0.38	0.89(4)	6
M(2)	0.31(2)	0.95(3)	1.38(4)	6	0.37	1.00(4)	6
M(2)	0.33(2)	0.97(4)	1.34(5)	6	0.36	0.96(6)	6
M(4)	0.57(1)	1.53(2)	2.27(4)	8	0.95	1.36(3)	6,8

ELECTRICAL PROPERTIES OF AMPHIBOLES

The electrical properties of a mineral govern its behavior in an applied electric field. The two main electrical properties are the *resistivity*, the reciprocal of the conductivity, which is a measure of the conduction current developed by an electric field, and the *dielectric constant*, a measure of the electrical polarization that occurs in an applied electrical field. There are very few studies of the electrical properties of amphiboles. Littler & Williams (1965) measured the conductivity of crocidolite along the fibre direction as a function of temperature. Typical results are summarized in Figure 109. Progressive oxidation resulted in systematically different behavior in repeated experiments; activation energies for conduction are 0.69(4) and 0.33(4) eV, respectively. Specific resistances for three samples were 10^9 ohm cm^{-1} for two samples of iron-rich crocidolite and 10^{10} ohm cm^{-1} for an iron-poor crocidolite. Conductivity across the fibre direction was found to be very low. Tolland (1973) performed similar experiments on a "hornblende" with an Fe/(Fe+Mg) ratio of ~0.19. The results are summarized in Figure 109; the activation energies found were 0.54 eV along *Z* and 0.57 eV along *Y*. Both studies suggested the conduction mechanism in amphiboles to be the electron-hopping process

$$Fe^{3+} + e^- \rightleftharpoons Fe^{2+}.$$